HHS Public Access

Author manuscript

Int J Min Sci Technol. Author manuscript; available in PMC 2018 April 09.

Published in final edited form as:

Int J Min Sci Technol. 2018 January ; 28(1): 43–51. doi:10.1016/j.ijmst.2017.12.013.

Analysis of monitored ground support and rock mass response in a longwall tailgate entry

G.S. Esterhuizen[a,*], **D.F. Gearhart**[a], and **I.B. Tulu**[b]

[a]NIOSH Pittsburgh Mining Research Division, Pittsburgh, PA 15236, USA

[b]West Virginia University, Morgantown, WV 26506, USA

Abstract

A comprehensive monitoring program was conducted to measure the rock mass displacements, support response, and stress changes at a longwall tailgate entry in West Virginia. Monitoring was initiated a few days after development of the gateroad entries and continued during passage of the longwall panels on both sides of the entry. Monitoring included overcore stress measurements of the initial stress within the rock mass, changes in cable bolt loading, standing support pressure, roof deformation, rib deformation, stress changes in the coal pillar, and changes in the full three-dimensional stress tensor within the rock mass at six locations around the monitoring site. During the passage of the first longwall, stress measurements in the rock and coal detected minor changes in loading while minor changes were detected in roof deformation. As a result of the relatively favorable stress and geological conditions, the support systems did not experience severe loading or rock deformation until the second panel approached within 10–15 m of the instrumented locations. After reaching the peak loading at about 50–75 mm of roof sag, the cable bolts started to unload, and load was transferred to the standing supports. The standing support system was able to maintain an adequate opening inby the shields to provide ventilation to the first crosscut inby the face, as designed. The results were used to calibrate modeled cable bolt response to field data, and to validate numerical modeling procedures that have been developed to evaluate entry support systems. It is concluded that the support system was more than adequate to control the roof of the tailgate up to the longwall face location. The monitoring results have provided valuable data for the development and validation of support design strategies for longwall tailgate entries.

Keywords

Longwall mining; Support; Tailgate; Monitoring; Coal mining

1. Introduction

Longwall gateroads are subject to significant changes in stress as the adjacent longwall panels are being retreat mined. The stress changes may include variation of the magnitude of the vertical and horizontal stress components as well as rotation of the major principal stress

*Corresponding author. eee5@cdc.gov (G.S. Esterhuizen).

directions. These stress changes can cause damage to the coal ribs and the rock mass surrounding a gateroad entry. Support systems to control the rock deformations have been developed over many years, and currently gateroad supports may consist of rock reinforcement using roof bolts and cable bolts, surface control using support channels and screen, and standing supports to control excessive roof and floor deformation [1,2]. Most support systems used today are developed through an empirical approach in which support systems are optimized to match the local geologic and stress conditions. The study presented in this paper is part of a research project being conducted by the Pitts-burgh Mining Research Division of the National Institute for Occupational Safety and Health (NIOSH) to develop engineering-based design procedures for gateroad support design.

The study was conducted at a longwall mine in West Virginia operating in the lower Kittanning coalbed at a depth of cover of 150–200 m. The coalbed thickness is about 1.5 m in the study area, but may be up to 2.4 m thick. In narrower seam conditions the mine will extract up to 1 m of shale roof rock during longwall extraction. The longwall district where the study was conducted consists of three longwall panels that are 365 m wide and are between 1500 and 2100 m long. The study site was located in the tailgate of the third panel to be mined in the district, shown in Fig. 1. For the purpose of discussing mining adjacent to the monitoring site, Panel 2B is the first panel to pass the site, and Panel 2C is the second panel.

Monitoring was initiated a few days after development of the gateroad entries and continued during passage of the longwall panels 2B and 2C on both sides of the entry. Measurements were conducted at a mid-pillar location of the entry as well as at an intersection location. Rock properties were obtained through uniaxial and triaxial strength tests conducted on rock cores collected from the monitoring site. Monitoring included overcore stress measurements of the initial stress within the rock mass, changes in cable bolt loading, standing support pressure, roof deformation, rib deformation, stress changes in the coal pillar, and changes in the full three-dimensional stress tensor within the rock mass at six locations around the monitoring site. The mid-pillar instruments were monitored up to 24 m inby the face, while the instruments at the intersection were terminated when the face reached the intersection. Fig. 2 is a sketch map showing the location of the instrumentation sites on the last day of monitoring. Visual records were kept of changes in rock and support conditions during the 13-month monitoring exercise. A detailed description of the monitoring system and a summary of results that were obtained from the study are provided in Gearhart et al. [3].

2. Geotechnical information

The immediate roof rocks of the lower Kittanning coalbed consist of dark gray to carbonaceous clay shale. The clay shale grades upward to gray sandy shale, dark-gray sandy shale, or gray sandstone. The gray sandy silt shale and dark-gray sandy silt shale beds vary in grain size and sand content, based on their proximity to the laterally correlative gray sandstone beds. Grain size and sand content decrease as the distance from the correlative sandstone beds increases. Stratigraphically located above this sandy zone is the Johnstown limestone, a lacustrine limestone of varying purity, which locally grades laterally to a claystone with calcareous nodules or flint clay. The Johnstown limestone is a regionally

recognized marker bed in the Allegheny Formation. The general overburden consists of alternating sandstone and shale beds with sandstone layers of between 10 and 20 m thick. The local geologic composition of the roof and floor, determined by core-drilling at the study site, is shown in Fig. 3. Inby the mid-pillar site the floor rolls downwards, and a slickensided joint extending across the entry was observed on the inby side of the mid-pillar site. These features indicate that the test site may be located on the margin of a paleochannel in the roof.

Laboratory testing of rock core was conducted to obtain geotechnical characteristics at the study site. Testing was conducted on core from the vertical holes in the roof and floor of the entry. In addition, core was tested from a 30° inclined hole drilled over the pillar adjacent to the study site. Laboratory tests consisted of uniaxial compressive strength testing, triaxial tests, and multistage triaxial tests. The compressive strength, elastic modulus, Poisson's ratio, and frictional and cohesive strength were obtained during this testing. The core from the inclined hole was used to determine shear strength along the bedding planes within the rock. Where rock samples were inadequate for compression testing, point load tests were conducted to supplement the results. Both axial and diametral point load tests were conducted. These tests were attempted to obtain a continuous strength record along the full length of the core, but this was not possible owing to the bedding breaks that occurred during core drilling and subsequent sample preparation. Only 30% of the recovered core was successfully cut, polished, and tested, indicating that most likely only the strongest sections of the core was tested. Table 1 summarizes the strength and mechanical properties of the rocks as tested.

Overcore stress measurements using hollow inclusion cells (HI-cells) were conducted to determine the initial stress conditions prior to the approach of the first longwall. Two measurements were made at depths of 8.0 and 8.5 m in a 30° inclined hole drilled into the roof strata over the solid coal on the panel side of the site. The results of the overcore measurements are presented in Table 2. The results confirmed the general east-west trend of the major horizontal stress observed in the eastern United States [4]. The major horizontal stress was slightly lower than the average predicted by the Mark and Gadde equation for eastern U.S. coal mines. The main development directions of the mine were designed to be oriented at about 45° to the major horizontal stress. Accordingly, the gateroads at the study site were developed in the direction N114W. The magnitude of the horizontal stress is sufficient to cause occasional roof-cutter formation during development. The cutters are typically located along the left corner of an entry advancing in the N114W direction, as expected.

It was interesting to note that during drilling of the 15-cm-diameter core hole for the overcoring measurements, the core was unbroken over the entire 9-m length. The core had to be broken mechanically by the driller to retrieve it after each drilling run. This is in contrast to the 30° inclined, 50-mm cored hole, which had 31 core breaks over its length, drilled through exactly the same strata as the 15-cm hole by an expert geotechnical drilling crew. This observation raises some questions about the usefulness of counting core breaks to characterize a bedded rock mass. The core breaks appear to be related to the drilling technique and do not necessarily indicate pre-existing breaks in the rock mass.

3. Mining and support

The instrumented entry was part of a three-entry gateroad system that serves two longwall panels. Looking inby, the panel on the right was mined first, followed by the panel on the left. The monitored entry serves as the tailgate of the second panel. The three entries are driven at 30.5-m centers, and crosscuts are driven at 45.7-m centers. Entry and crosscut development is 5.5 m wide. And primary roof support consists of a row of four 1.8-m-long by 19-mm-diameter roof bolts with a single 1.2-m-long resin cartridge spaced 1.2 m apart; the secondary support was a pair of 3.0-m by 17-mm cable bolts with two resin cartridges installed through a strap every 2.4 m. Secondary support is installed about 20–30 m behind the advancing face. In addition, there were bolts installed at a 45° angle at the corner of the rib and roof on 2.4-m spacing.

In the study section, standing supports in the form of two rows of nine-point wooden cribs were installed after the first panel had been mined. The nominal crib dimensions were 90-cm by 90-cm wide and were installed to the full height of mining which was 2.1 to 2.4-m high. The standing support system was required to maintain stable ground conditions up to the advancing longwall face, and provide an adequate opening along the edge of the gob, inby the shields, to allow ventilation to flow to the first crosscut inby the face.

Mining of the first longwall panel adjacent to the site (Panel 2B in Fig. 1) commenced on November 30, 2015, and passed by the instrumented site on February 9, 2016, after some 770 m of face advance. The panel was completed on May 26, 2016, with a total panel length of 2325 m. Mining of the second panel (Panel 2C in Fig. 1) commenced on June 19, 2016, advancing 520 m to reach the mid-pillar study site on July 30, 2016. Monitoring of the instruments continued until the face had advanced up to the crosscut site on August 1, 2016. At this stage the mid-pillar site was located about 24 m inby the face, and most of the data loggers were still recording useful data.

3.1. Instrumentation

The initial pre-mining stress was measured by overcoring of two hollow inclusion cells in the same hole. Subsequent stress changes were measured by long-term monitoring of six hollow inclusion cells located in six different holes of the roof strata on both sides of the entry. Instrument locations at the mid-pillar site are shown in Fig. 4. Roof rock deformation was measured using 2.4-m-long wire extensometers with multiple measuring points. In addition, a 6.0-m-long multiple-point wire extensometer was installed at the center of each monitoring site. Support performance was measured by installing load cells underneath the face plates of the cable bolts at the time of installation. Cable bolt load cells were installed between 20 and 30 m outby the advancing heading. At this time, the extensometers were also installed. Within the coal pillar, deformation of the coal rib was monitored using a multiple-point extensometer while stress changes in the coal were measured using three borehole pressure cells. Wiring-up and data recording started a few days later when the area became less congested by mining equipment. A detailed discussion of the instrumentation program is presented in Gearhart et al. [3].

The nine-point (9-pt) wood crib loading was monitored using flat-jack load cells that were located near the top of the cribs. Roof-to-floor deformation was measured using a wire potentiometer that measured the distance between two nails driven into the timber near the top and bottom of each crib.

Visual observations and mapping of rock conditions were made on several occasions during the study period. The observations mainly focused on changes in rock conditions in the roof, ribs, and floor of the excavations. Electronic data loggers were used to record all the instruments for the duration of the study.

4. Results

The monitoring results of the mid-pillar site are evaluated and discussed here. The intersection appeared to be much more stable than the mid-pillar site, with much less deformation measured and less loading of the cable bolt and standing supports. Further investigation is currently ongoing to determine the likely cause of this unexpected behavior. The intersection site results will, therefore, not be discussed.

4.1. Stress changes measured

The hollow inclusion cells measured the stress changes as the first and second panels were mined. Fig. 5 shows how the horizontal components of the stress, measured by the HI-cells located in the 60° holes, were rotated as the second longwall approached the instrumented site. The orientation of the major stress tended to rotate towards the direction of the entry, but did not become fully parallel to the entry. The HI-cell located on the panel side of the entry was able to record stress changes over the gob, showing that the major horizontal stress magnitude increased to 10.6 MPa at this location about 8 m above the coal seam.

The stress changes experienced by the rock surrounding the entry were plotted as a stress path, shown in Fig. 6. Fig. 6 plots the change in the vertical stress against the change in the horizontal stress component perpendicular to the entry direction. The location of the two longwall faces at critical times is shown in Fig. 6. When the first panel passed, the entry experienced a small reduction in horizontal stress, while the vertical stress increased by about 1.4 MPa. A gradual increase in both the horizontal and vertical stress continued over the months that the first panel was mined to its limit. During this time, minor deterioration of rib conditions was observed in the entry. Continuous roof deformations of about 3 mm were also measured by the roof extensometers. When the second panel approached, there was an initial rapid increase in the vertical stress, followed by an increase in the horizontal stress after the longwall face had passed the monitoring site. Overall, the average vertical stress increased by about 6.2 MPa, ending at about 2.6 times the cover stress, while the horizontal stress increased to about 1.3 times the pre-mining value. When the second longwall face was located about 1.8 m outby the mid-pillar site, the average vertical stress was about 2.2 times the initial vertical stress.

As noted in Fig. 6, stress components are calculated in a vertical plane perpendicular to the long axis of the entry.

4.2. Entry deformation

Deformation of the entry was measured using a total of nine multiple-point roof extensometers. During passing of the first longwall panel, the roof in the mid-pillar section responded by sagging between 3 and 15 mm as recorded by seven of the nine extensometers. Two of the extensometers did not provide consistent results. During the mining of the remainder of the first panel, a low rate of roof deformation was observed, further sagging by approximately 3 mm.

Roof sag measurements associated with the approach of the second face are shown in Fig. 7. When the second panel approached within about 23 m of the monitoring site, the average roof sag accelerated and achieved about 40 mm when the face was 1.8 m inby the monitoring site. When the face reached the monitoring site, the average roof sag was approximately 40 mm, increasing to about 90 mm when the measuring site was 24 m inby the face. At this stage the extensometer readings became irregular as the limit of the instruments were met. The data recorders were removed at this time as the longwall face reached the crosscut monitoring site.

As noted in Fig. 7, negative distances indicate the site is outby the longwall face.

Vertical roof sag measured by the extensometers installed above the roof line is shown in Fig. 8 when the longwall face was 1.8 m inby the monitoring site. The roof displacements were highly variable between the seven different extensometers. The average roof deflection was about 40 mm at this time. It can be seen that the majority of the roof deformations occurred below the 2.4-m mark.

4.3. Observed ground conditions

After development and prior to mining of the two longwall panels adjacent to the monitoring site, the roof conditions in the No. 1 entry were assessed to be good with minor spalling occurring behind the steel screen support shown in Figs. 9 and 10. No sign of excessive load was observed by inspection of roof bolt and cable bolt plates. This was also confirmed by the monitored cable bolt loads. The ribs had deteriorated mainly because the claystone floor was exposed below the coal, which appeared to flake and induce tensile cracks in the coal. Slabs of coal fell from the ribs and formed a rubble pile along the panel side of the entry. The pillar side rib appeared to be more stable, which may be attributed to the rib bolt support installed along the pillar side. The floor was solid and did not show signs of cracks or heave. There was no ground water present, although some water was intersected when a 15-m up-hole was core drilled for rock strength testing. This hole was plugged to prevent water ingress.

As indicated in Fig. 9, the left rib is the future second panel that will be mined, and the right rib is a 30.5-m-wide pillar.

As noted in Fig. 10, the crosscut is to the left of the image; some of the instrumented cable bolts and extensometers are visible in this photo, with the monitoring cable bundle running into the crosscut.

Ground conditions remained essentially unchanged over the majority of the monitoring period. There was a slow deterioration of the ribs, which appeared to be associated with the spalling of the floor claystone that was exposed along the lower 30–60 cm of the ribs. Some of the pillar corners fell away or developed cracks during this period. The crosscut roof deteriorated after the first panel had passed, and additional timber posts were installed to secure safe access to the data recorders.

The entry roof appeared to be remarkably stable until the long-wall face approached within about 50 m, upon which spalling started to occur along the roof-rib contact. The roof extensometers did not respond to this initial spalling, only showing roof sag when the face was about 23 m inby. As the longwall panel approached within about 24–30 m, the spalling developed into cutters and the cutter formation was more severe on the pillar side than on the panel side of the entry. The cutter on the pillar side progressed upwards to approximately 30 cm above the roof line at the long-wall face position. On the panel side of the entry the cutter was not as severe, manifesting as minor spalling, and only developing to about 15 cm above the roof line at the longwall face position.

The ribs continued to spall, losing about 30 cm of material at the longwall position. The floor started to develop floor cracks and heave only within 15–23 m of the longwall face. Floor heave was minor and was visually estimated to be no more than 10–15 cm. Some of the center timber-crib slabs were still loose at about 20 m outby the advancing face, indicating that insignificant loads were being transferred to the cribs at this stage. It was only when the cribs were located right at the longwall face that one could observe signs of loading and biting-in of the timbers. At this stage the average roof sag was about 45 mm and floor cracks were present.

From the longwall face position the roof was visible for about 20 m inby the tailgate corner. The roof was visibly sagging, and compression of the cribs was becoming obvious. The gob was forming immediately behind the shields in a controlled manner and did not overrun the row of cribs adjacent to the gob. The screen was able to hold the roof together and successfully prevented roof unraveling as far as could be seen. The grouted and cable bolts were all in-place within the range of visibility, and none of them appeared to have fallen out of the roof. Rubble from rib spalling obscured the floor; therefore no comments can be made about floor heave inby the face.

From a ventilation point of view, the support system was successful in maintaining an opening for airflow to the first crosscut inby the face.

4.4. Response of the cable bolts

The response of the cable bolts and the crib standing supports is of particular interest at the tailgate/face corner and inby the face in providing safe ground conditions and in meeting ventilation requirements. At the mid-pillar monitoring site, the support performance and ground response were monitored up to 24 m inby the advancing longwall face, and will be discussed here.

The cable bolt response against the average roof sag measured by the extensometers is shown in Fig. 11. Fig. 11 shows that there is a large variability in cable bolt responses. The majority of the cable bolts were loaded between 50 and 100 kN when monitoring started a few days after installation. This initial load is attributed to the thrust of the roof bolting machine and roof deformation prior to the start of data recording. Two of the cable bolts had initial loads of 175 and 200 kN, which are unexpectedly high.

As is evident in Fig. 11, the red dashed line is the average cable bolt response.

The averaged peak load of the individual cable bolts was 245 kN, which is close to the expected peak breaking strength of 260 kN. The individual cable bolt peak loads varied from about 190–320 kN. The individual peak loads occurred for roof sag values from 60 to 90 mm. All of the cable bolts had shed load when the roof sag exceeded 90 mm.

Fig. 11 also shows the averaged load response of the cable bolts against roof sag. The average peak load is lower at 216 kN because all of the bolts did not reach their peak load simultaneously. The average peak load is achieved at 70 mm of roof sag. The average stiffness of the cable bolts was estimated using the slope of the average load/sag curve. The average stiffness is approximately 2.3 kN/mm taken between the 16 and 70-mm roof sag points. This is considerably lower than the typical stiffness of 3.6 kN/mm measured in controlled tests [5].

It may be questioned whether the cable strands were actually failing or whether some other mechanism, such as grout failure, was causing the load shedding of the cable bolts. The monitoring results did show progressive loss of load which appears to be related to individual cable strands failing, one strand at a time. Fig. 12 shows failure of each of the seven strands of one of the cable bolts and failure of five strands of a second cable bolt.

4.5. Load sharing between cable bolts and standing supports

Of particular interest in the monitoring study was to establish how load is shared between the cable bolts and the standing supports. Fig. 13 shows the average crib loading and the average cable bolt loads against their location, relative to the advancing longwall face. In this chart, the cable bolt loads are averaged separately for the four bolts inby and four bolts outby the monitored cribs. The initial loading of the outby set of cable bolts was greater than the loads on the inby set. When the face reached the instrumented site, the average cable bolt loads were around 150–170 kN, which is about 50%–60% of their ultimate breaking strength. The average crib load was about 125 kN, which is only about 18% of their typical design capacity of 670 kN. At this stage the roof was fully under control of the support system.

In Fig. 13, negative distances indicate that the longwall face is inby the monitoring site.

As the advancing longwall face advanced outby the instrumented site, roof sag increased rapidly and the support loads increased significantly. The cable bolts achieved their peak loads when they were located about 8 m inby the longwall face. At this stage the load on the cribs started to increase rapidly as some of the cable bolts started to shed load. When the instrumented site was 24 m inby the face, the average crib load was 380 kN and most of the

cable bolts had failed or had shed significant load. The results indicate that the standing supports were only lightly loaded up to the tailgate corner. They only started to attract meaningful loading when they were located inby the face, after the cable bolts had started to shed load. Overall, the support system was considered to be performing well since the ventilation requirements were met and controlled conditions were maintained at the tailgate corner.

5. Application of monitoring results to validate numerical models

The field monitoring results are very useful for validating the numerical models that are being developed at NIOSH to assist with ground support design in gateroads. A numerical model of the mid-pillar site was created to simulate the entry under the loading conditions measured prior to longwall panel extraction. The load on the boundaries of the model was increased to follow the stress loading path shown in Fig. 6, up to the point when the advancing longwall face was 1.8 m inby the monitoring site. The model results were evaluated to determine how well the modeling procedures would predict the observed rock response and support performance. The model was then subjected to increasing load to achieve deformations similar to those observed when the longwall face had passed the monitoring site. Of particular interest was to establish whether the numerical model would correctly predict the load response and load shedding of the cable bolts under large roof deformations.

5.1. Model layout and analysis approach

The numerical models are created using the FLAC3D finite difference software [6]. Each model represents a slice taken at right angles to the long axis of the entry being modeled, shown in Fig. 14. The thickness of the slice is set to equal the support row spacing along the length of the entry. In this way, a semi-two-dimensional model is achieved, with correctly modeled supports. The bedded strata is modeled using the strain-softening, ubiquitous joint constitutive model available in FLAC3D. The rock matrix within the bedded units is modeled as intact rock, with 58% strength reduction to account for the scale effect when going from laboratory test scale to field-scale rock [7,8]. Areas of low confinement, in which delamination of bedded strata and extensional fracturing may occur, are modeled using an adoption of the cohesion-weakening, friction-hardening (CWFS) approach [9–13]. Confinement-dependent dilation is implemented using the approach of Alejano and Alonso [14]. The rock strength data shown in Table 1 was used as a starting point for developing model inputs. The details of the procedures for estimating the field-scale rock strength and bedding shear strength are described in Esterhuizen and Esterhuizen et al. [15,16]. Initial stress in the model was based on the overcore stress measurements taken at the experimental site.

Fig. 14 indicates that the detail plot shows supports installed within the model and detail of rock layering and ground supports in the roof.

Solid bar roof bolts and cable bolts are modeled using the builtin finite element structures available in FLAC3D. Supports are modeled using the actual strength and yield properties provided by the manufacturers. Grouted bolts are modeled as untensioned steel units,

attached to the grout and surrounding rock at nodes that are 10 cm apart. This has been found to satisfactorily model both the elongation and shear loading of the bolts. Grout strength is based on the results of short-encapsulation tests. The models allow grout bond strength to decay as the bolts become debonded and shear at the grout-rock interface. The typical “grip factor” used for modeling the grouted bolts is 520 kN/m. Cable bolts are modeled similarly to the grouted bolts, with a reduction in the modulus of the steel to emulate the lower stiffness associated with the cable unwinding at increasing load. The cable bolt stiffness was initially set to 3.6 kN/mm as determined by controlled tests, for example Tadolini et al. [5]. After completing the initial model analyses, it was found that the modeled cable bolts were too stiff compared to the measured field results. In the final models, the cable bolt stiffness and peak strength was modified to match the averaged field results. Fig. 15 shows the calibrated cable bolt response compared to the field-measured response. This result was achieved by continuing to load the model entry until the roof sag exceeded 90 mm and the modeled cable bolt had failed. The key parameters for achieving the calibration were determined by setting the apparent modulus of the steel cable to 27 GPa. Ultimate yield strain was maintained at 3.5% over a 60-cm cable length. The model results presented below were obtained by using the calibrated cable bolt parameters.

5.2. Comparison between numerical model response and field results

The numerical model results are compared to the field monitoring data for the final stages of the entry monitoring study, when the second longwall panel approached and mined up to 1.8 m outby the monitoring site. The situation after the longwall face had mined past the monitoring site was not modeled because of the complex geometry and rock behavior that resulted from the extraction of coal on one side of the entry and the subsequent formation of the gob.

Fig. 16a shows the rock mass and support response predicted by the numerical model for the stage when the monitoring site was located 23 m outby the approaching second longwall face. Fig. 16a shows the various modes of rock damage as: (1) bedding shear (shear failure of ubiquitous joints); (2) delamination (tensile failure of bedding joints); (3) extension fractures (extension failure of rock material under low confinement); (4) matrix shear (rock material shear failure under confined conditions); (5) residual shear (sheared rock now at residual strength); and (6) tensile fractures (tensile failure of rock material). At this stage the roof was mainly impacted by delamination along bedding planes, with some spalling indicated above the entry corners. Some coal spalling was predicted near the floor where the floor claystone was exposed. Cable bolts loads had not changed much since installation with loads at about 65–90 kN. The roof deflection at the center span of the model was 6 mm at this stage, which is very similar to the average monitored roof sag of 10 mm, shown in Fig. 7.

Fig. 16b shows the modeled entry conditions for the stage when the longwall face had approached to 1.8 m inby the monitoring site. At this point the rock damage was much more extensive, and the cable bolt loads increased to about 130–155 kN, which is very similar to average loads measured by the cable bolt load cells. This indicates that the calibrated cable bolt model is performing as desired.

Fig. 17 shows the numerical model calculated roof deformations within the entry roof at the loading stage, corresponding to the longwall face being 1.8 m inby the monitoring site. The results can be compared to Fig. 8, which shows that the model-predicted deformations are very similar in magnitude and distribution when compared to the monitored results. The average roof sag at the roof line is 40 mm in both the model and the field-monitored data.

6. Conclusions

An extensive field monitoring study was conducted by NIOSH in which the rock mass and support response was measured in a longwall mine gateroad at a depth of cover of 180 m. The results demonstrated that the support system was more than adequate to control the ground conditions up to the longwall tailgate corner. It was only when the longwall face had passed outby the monitoring site that the support system started to become overloaded. The cable bolts started to shed load when they were located some 8 m inby the face, and all the monitored cable bolts had shed load when the monitoring site was 24 m inby the face. The standing supports carried only a limited load of about 120 kN each when they were located at the tailgate corner. It was only after the cable bolts started shedding load that the standing supports became significantly loaded, with loads increasing to 350 kN when the data loggers were removed.

The monitoring results were used to validate numerical modeling procedures that are being developed to assist with coal mine support design. These monitoring results were also used to calibrate the cable bolts defined in the model to better match the field-monitored results. After modifying the modeled cable bolt parameters, it was possible to achieve satisfactory cable bolt response, including the simulation of cable bolt failures after approximately 75 mm of roof sag. The calibrated model provided realistic rock failure and deformation results, closely following the monitored outcomes.

The study has provided significant insight into the response of the rock mass and support to the changing loads imposed by an advancing longwall. The results have contributed to understanding support system behavior in the extreme loading conditions at a longwall tailgate corner.

7. Disclaimer

The findings and conclusions in this report are those of the authors and do not necessarily represent the views of the National Institute for Occupational Safety and Health. Mention of any company or product does not constitute endorsement by NIOSH.

References

1. Batchler T. Analysis of the design and performance characteristics of pumpable roof supports. Int J Min Sci Technol. 2017; 27(1):91–9. [PubMed: 28775910]
2. Barczak, TM. A retrospective assessment of longwall roof support with a focus on challenging accepted roof support concepts and design premises. Proceedings of the 25th International Conference on Ground Control in Mining; Morgantown, WV. p. 232-343.

3. Gearhart, D., Esterhuizen, G., Tulu, I. Changes in stress and displacement caused by longwall panel retreats. Proceedings of the 36th International Conference on Ground Control in Mining; SME. Morgantown, WV: ICGCM; 2017. p. 313-20.

4. Mark, C., Gadde, M. Global trends in coal mine horizontal stress measurements. Proceedings 27th International Conference on Ground Control in Mining; Morgantown: WV University; 2008. p. 319-31.

5. Tadolini, CS., Tinsly, J., McDonnell, JP. The next generation of cable bolts for improved ground control. Proceedings of the 31st International Conference on Ground Control in Mining; ICGCM. Morgantown, WV: West Virginia University; 2012. p. 27-34.

6. Itasca Consulting Group. FLAC3D fast lagrangian analysis of continua in 3 dimensions. Minneapolis: Itasca Consulting Group; 2014.

7. Gale, WJ., Mark, C., Oyler, DC., Chen, J. Computer simulation of ground behaviour and rock bolt interaction at Emerald Mine. Proceedings of the 21st International Conference on Ground Control in Mining; Morgantown, WV: West Virginia University; 2004. p. 27-34.

8. Hoek, E., Brown, ET. Underground excavations in Rock. London: Institution of Mining and Metallurgy; 1980. p. 525

9. Stacey TR. A simple extension strain criterion for fracture of brittle rock. Int J Rock Mech Min Sci Geomech Abstr. 1980; 18(6):469–74.

10. Martin CD, Kaiser PK, McCreath DR. Hoek-Brown parameters for predicting the depth of brittle failure around tunnels. Can Geotech J. 1999; 36(1):136–51.

11. Diederichs, MS., Carvalho, JL., Carter, TG. A modified approach for prediction of strength and post yield behaviour for high GSI rock masses in strong brittle ground. Proceedings from the 1st Canada-US Rock Mechanics Symposium; p. 249-57.

12. Kaiser PK, Amann F, Steiner W. How highly stressed brittle rock failure impacts tunnel design. Eurock. :27–38.

13. Esterhuizen, GS., Tulu, IB., Bajpayee, TS. Application of a Brittle Failure model to assess roof stability in coal mine entries. Proceedings 51st US rock mechanics/geomechanics symposium; American Rock Mechanics Association; 2017. p. 17-444.

14. Alejano LR, Alonso E. Considerations of the dilatancy angle in rocks and rock masses. Int J Rock Mech Min Sci. 2005; 42(4):481–507.

15. Esterhuizen, GS. A stability factor for supported mine entries based on numerical model analysis. Proceedings of 31st International Conference on Ground Control in Mining; Morgantown. 2012. p. 9

16. Esterhuizen, GS., Bajpayee, TS., Ellenberger, JL., Murphy, MM. Practical estimation of rock properties for modeling bedded coal mine strata using the Coal Mine Roof Rating. 47th US rock mechanics/geomechanics symposium; American Rock Mechanics Association; 2013.

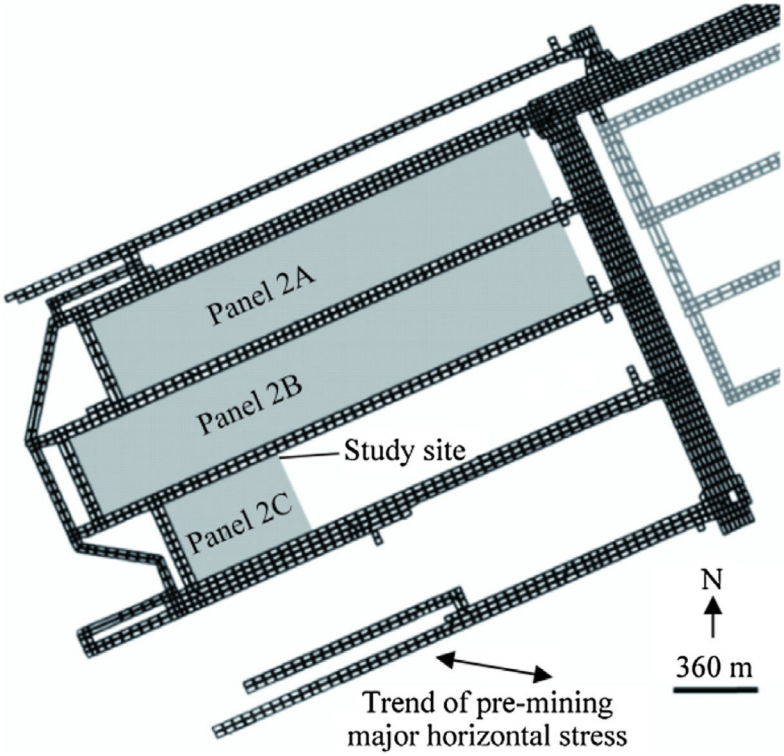

Fig. 1.
Layout of longwall panels and location of study site.

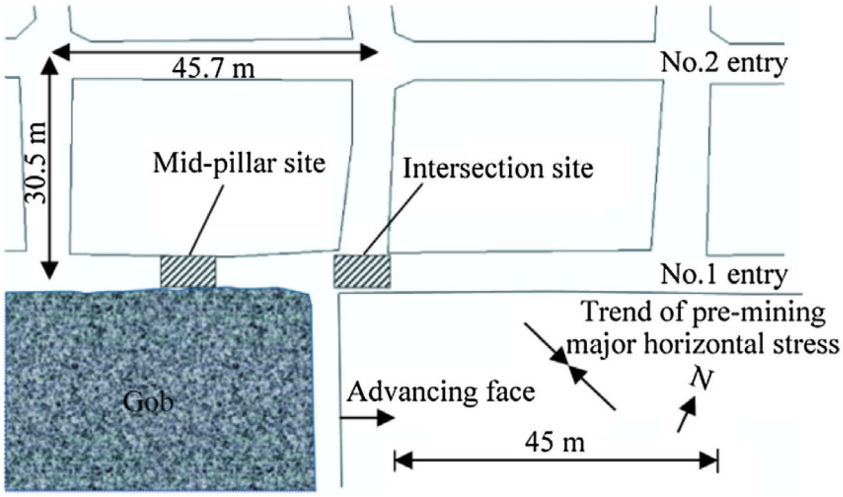

Fig. 2.

Detail view of location of monitoring sites in the No. 1 (tailgate) entry of the longwall, showing longwall face position at the end of the monitoring period.

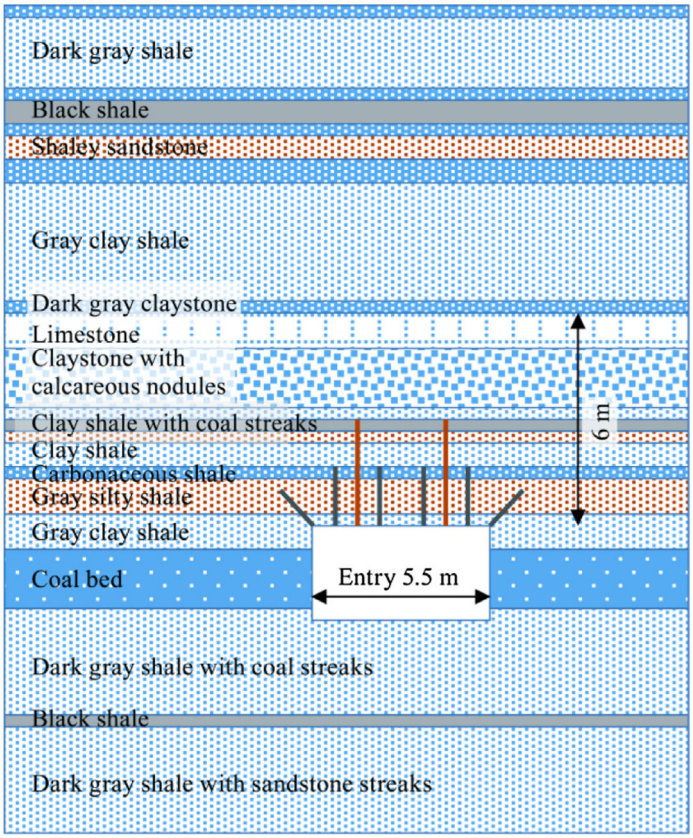

Fig. 3.
Section showing geologic layering and location of entry and support system.

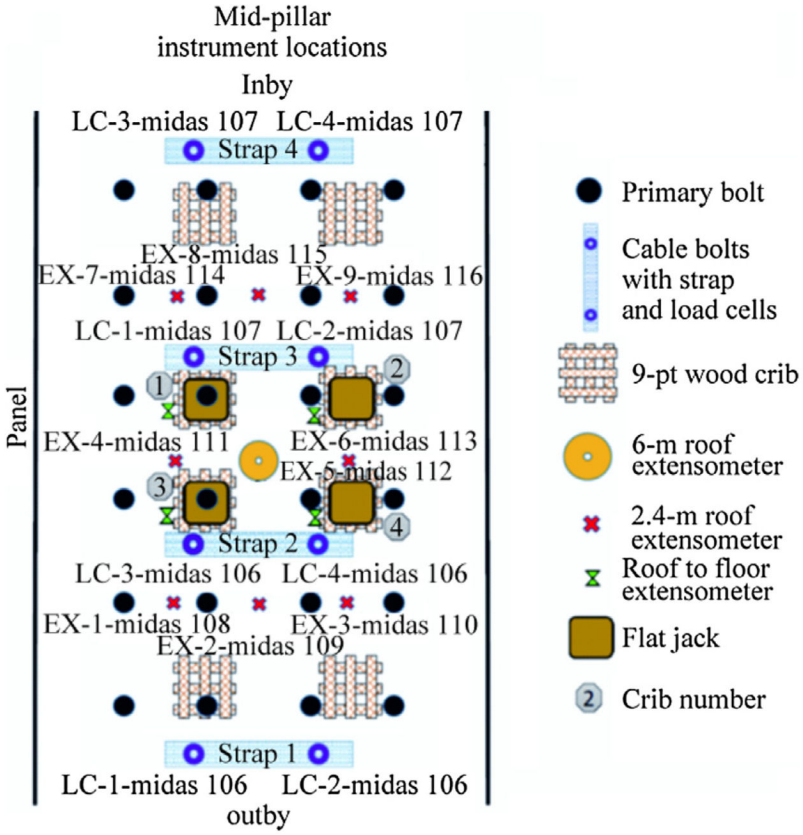

Fig. 4.
Instrument types and locations at the mid-pillar site.

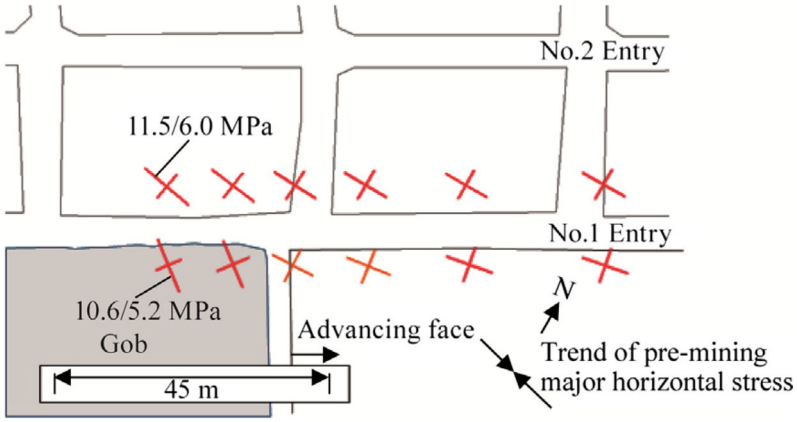

Fig. 5.

Plot showing principal stress orientations and magnitudes in the horizontal plane, measured by the two HI-cells located 8 m above the roof of the entry in the holes drilled at an inclination of 60°.

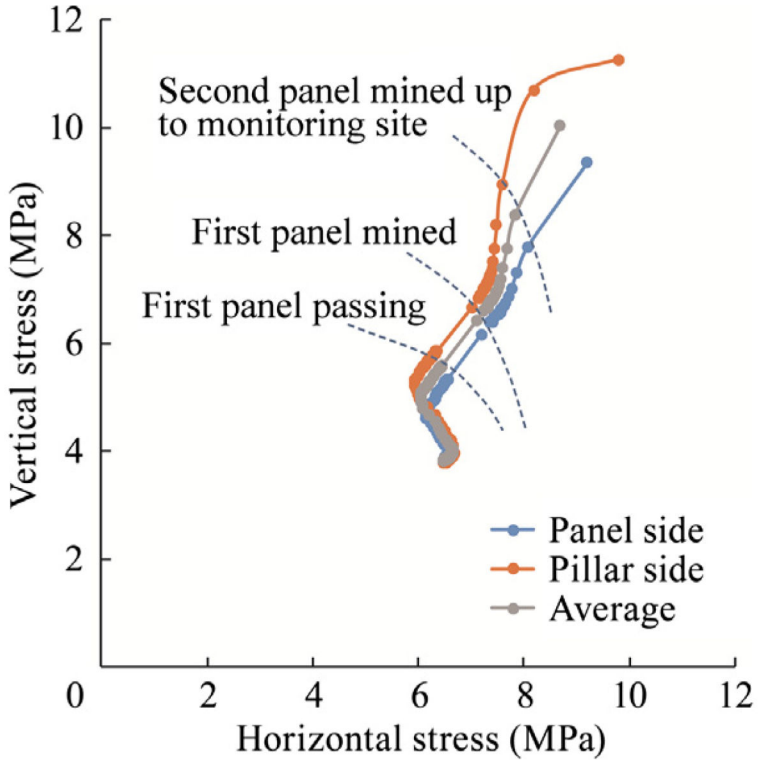

Fig. 6.
Stress path experienced by the No. 1 entry.

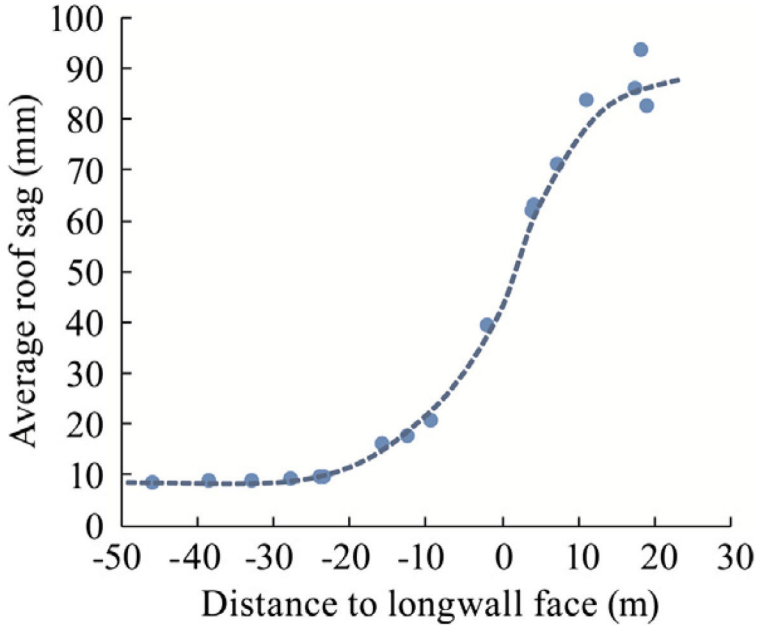

Fig. 7.

Average roof sag measured by seven extensometers at the mid-pillar site versus distance to the advancing longwall face.

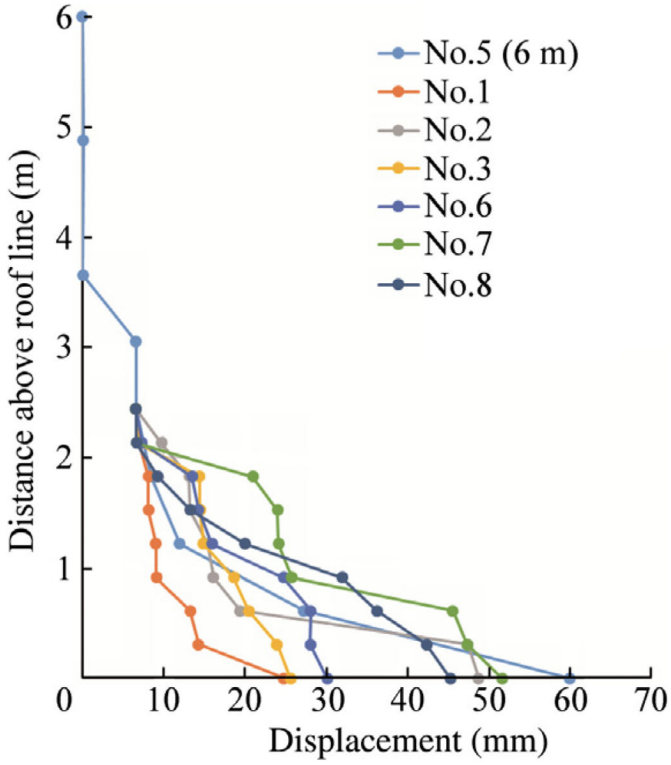

Fig. 8.

Vertical roof deformation measured by extensometers when the longwall face was 1.8 m inby the center of the mid-pillar site.

Fig. 9.
Ground conditions in Entry No. 1 looking inby from the mid-pillar site prior to mining of the first panel.

Fig. 10.
Roof conditions in Entry No. 1 at the crosscut site prior to mining of the first panel.

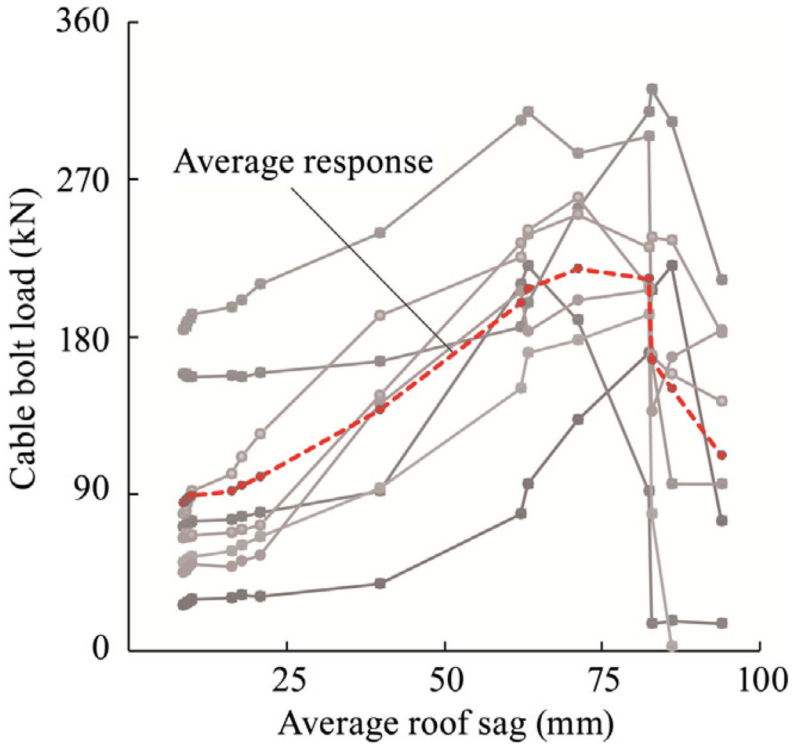

Fig. 11.
Response of individual cable bolts versus roof sag shown as gray lines.

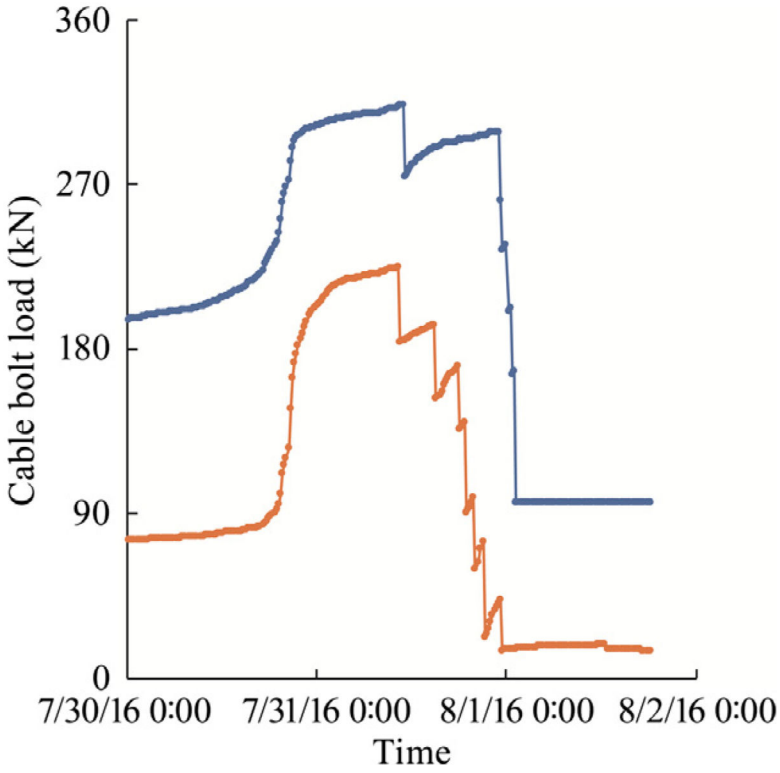

Fig. 12.
Cable bolt monitoring results showing load increase and failure of individual steel strands.

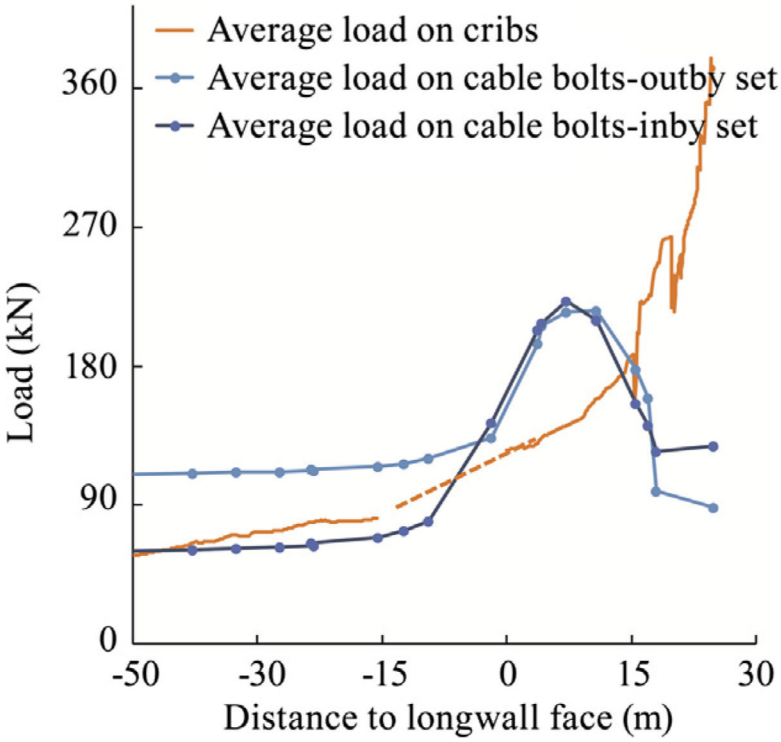

Fig. 13.

Average response of crib supports and two sets of cable bolts against distance to the advancing longwall face.

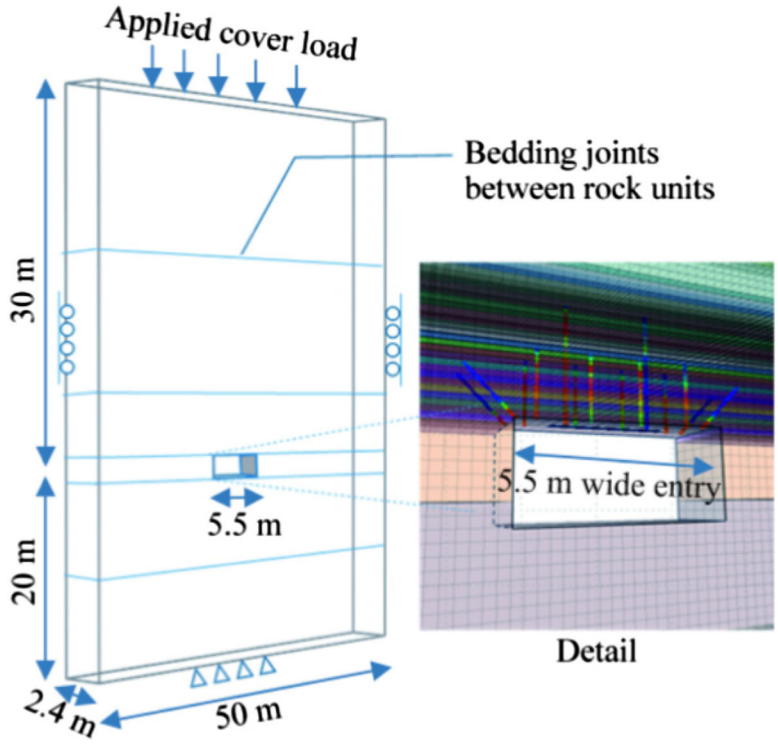

Fig. 14.
Sketch showing a typical model used to simulate a coal mine entry.

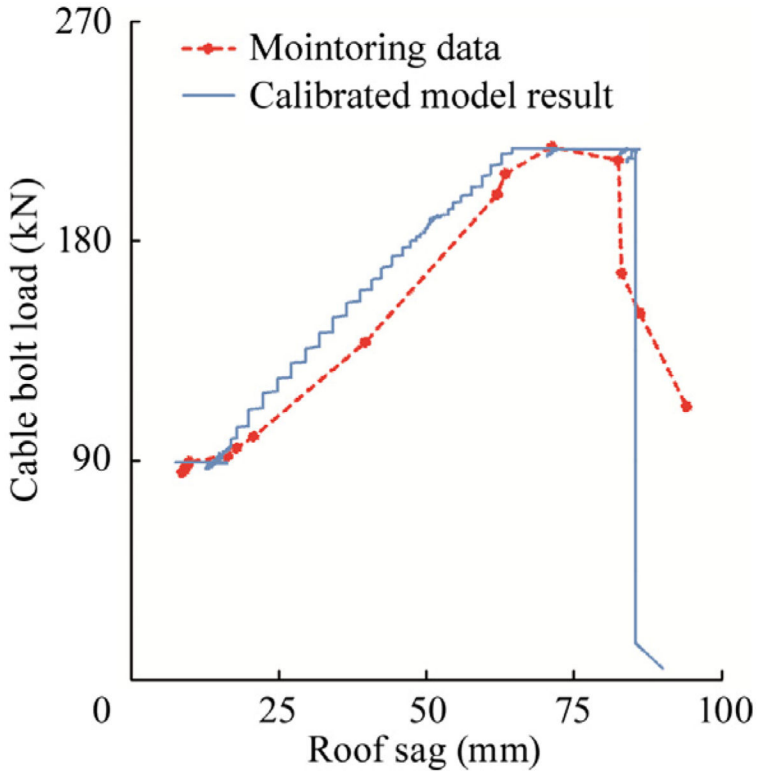

Fig. 15.

Comparison of cable bolt response obtained from a calibrated numerical model and from the averaged field monitoring results.

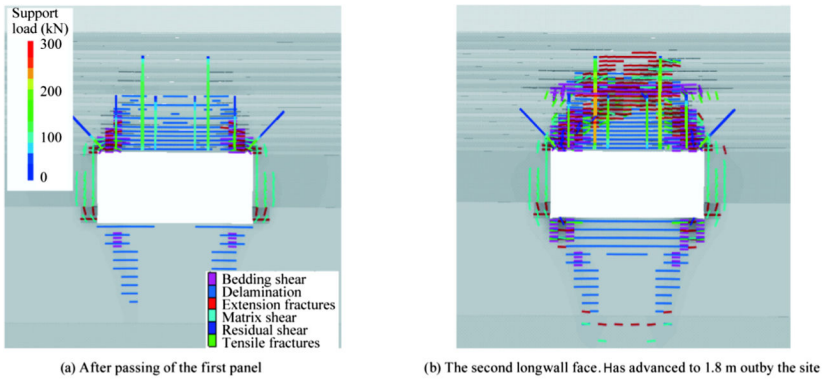

Fig. 16.

Model results for the mid-pillar site showing rock mass damage and support response:

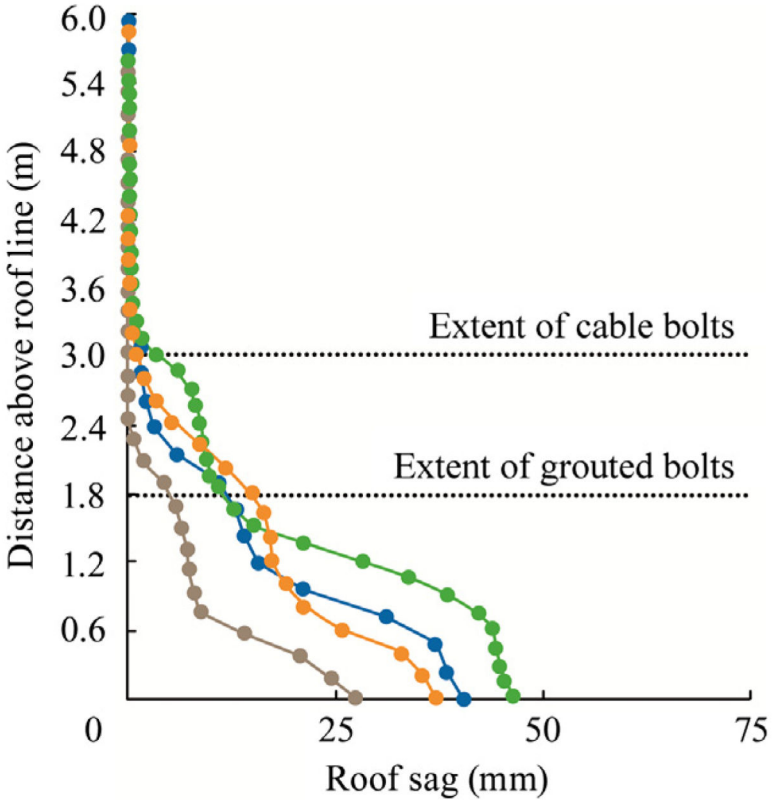

Fig. 17.

Roof sag predicted by numerical model at four locations across the mid-pillar site when the longwall face was located 1.8 cm outby the site, in compare with Fig. 8.

Table 1

Summary of rock strength properties, loosely correlated top-down to Fig. 3.

Rock type	UCS (MPa)	Elastic modulus (GPa)	Poisson's ratio	Internal friction angle (°)	Residual friction angle (°)
Dark gray shale	85.3	16.7	0.15	24.00	56.0
Black shale	22.7				
Shaley sandstone	144.0	40.8	0.25	19.20	40.5
Gray clay shale	80.8	15.5	0.26		34.4
Limestone	265.0	78.6	0.30	33.10	
Claystone with calcareous nodules	103.6	22.3	0.14	18.10	42.4
Clay shale	43.8	14.1	0.22	31.00	39.3
Gray silty shale	58.5	10.8	0.21	26.40	35.2
Coalbed being mined	N/A				
Dark-gray shale with coal streaks	59.0	9.4	0.28	7.65	54.7
Dark-gray shale with sandstone streaks	60.7	16.0	0.14	14.30	41.4

Table 2

Overcore stress measurement results.

Hole depth	Stress component	Stress (MPa)	Dip (°)	Azimuth (°)
8.0 m	Major	6.52	13	117
	Intermediate	5.47	12	210
	Minor	4.14	72	342
8.5 m	Major	8.28	4	290
	Intermediate	6.58	5	21
	Minor	4.48	83	165